Development 137, 249-259 (2010) doi:10.1242/dev.040782

Tgif1 and Tgif2 regulate Nodal signaling and are required for gastrulation

Shannon E. Powers[1,*], Kenichiro Taniguchi[1,*], Weiwei Yen[2], Tiffany A. Melhuish[1], Jun Shen[3], Christopher A. Walsh[3], Ann E. Sutherland[2] and David Wotton[1,†]

SUMMARY

Tgif1 and Tgif2 are transcriptional co-repressors that limit the response to TGFβ signaling and play a role in regulating retinoic-acid-mediated gene expression. Mutations in human *TGIF1* are associated with holoprosencephaly, but it is unclear whether this is a result of deregulation of TGFβ/Nodal signaling, or of effects on other pathways. Surprisingly, mutation of *Tgif1* in mice results in only relatively mild developmental phenotypes in most strain backgrounds. Here, we show that loss-of-function mutations in both *Tgif1* and *Tgif2* result in a failure of gastrulation. By conditionally deleting *Tgif1* in the epiblast, we demonstrate that a single wild-type allele of *Tgif1* in the extra-embryonic tissue allows the double null embryos to gastrulate and begin organogenesis, suggesting that extra-embryonic Tgif function is required for patterning the epiblast. Genetically reducing the dose of *Nodal* in embryos lacking all Tgif function results in partial rescue of the gastrulation defects. Conditional double null embryos have defects in left-right asymmetry, which are also alleviated by reducing the dose of Nodal. Together, these data show that Tgif function is required for gastrulation, and provide the first clear evidence that Tgifs limit the transcriptional response to Nodal signaling during early embryogenesis.

KEY WORDS: Nodal, TGF beta, Tgif, Gastrulation, Transcription, Mouse

INTRODUCTION

Transforming growth factor (TGF) beta family signaling is initiated by the binding of specific ligands to cell surface receptor serine/threonine kinases (Heldin et al., 1997; Massagué, 1998; Massagué et al., 2005). Following phosphorylation by the type II receptor, the activated type I receptor phosphorylates specific receptor-activated Smad (R-Smad) proteins. The predominant R-Smads activated in response to signals from TGFβ, activin (inhibin beta – Mouse Genome Informatics) and Nodal are Smad2 and Smad3. Phosphorylated R-Smads form complexes with Smad4, accumulate in the nucleus and activate gene expression, in part by recruiting specific transcriptional coactivators, including p300/CBP (Massagué et al., 2005). Inhibitor molecules act at almost every stage of the signaling pathway (Itoh and ten Dijke, 2007), and once Smads enter the nucleus, specific transcriptional co-repressors limit the response to TGFβ (Wotton and Massague, 2001).

Tgif1 is a transcriptional co-repressor for TGFβ-activated Smads, which competes with coactivators for Smad interaction and recruits general transcriptional co-repressors, thereby limiting the transcriptional response to TGFβ signaling (Wotton et al., 1999a). Tgif2 shares a conserved C-terminal repression domain with Tgif1, and can function as a Smad co-repressor in cultured cells (Imoto et al., 2000; Melhuish et al., 2001). Both Tgif1 and Tgif2 interact with the mSin3/HDAC co-repressor complex, and Tgif1 also recruits CtBP co-repressors (Melhuish et al., 2001; Melhuish and Wotton, 2000; Melhuish and Wotton, 2006; Sharma and Sun, 2001; Wotton et al., 1999b). Tgif1 can also repress gene expression via interaction with the RXR nuclear receptor, and may limit transcriptional activation by retinoic acid receptors when ligand is limiting (Bartholin et al., 2006; Bertolino et al., 1995).

Mutations in human *TGIF1* are associated with holoprosencephaly (HPE), a severe genetic disease affecting craniofacial development (Gripp et al., 2000). However, it is not known how loss-of-function mutations in human *TGIF1* cause HPE, and in a mixed strain background, targeted mutations in mice have not revealed a clear role for Tgif1 during embryogenesis (Bartholin et al., 2006; Jin et al., 2006; Mar and Hoodless, 2006; Shen and Walsh, 2005). On a more pure C57BL/6J background a proportion of *Tgif1* null animals die perinatally, but we have not observed HPE in these mice (Bartholin et al., 2008). An additional *Tgif1* mutation, which may be hypomorphic, has been found to cause anterior defects in a strain-specific manner (Kuang et al., 2006). Although there is no evidence for mutations in the human *TGIF2* gene being associated with HPE, it is clearly possible that these two related proteins share overlapping function during embryogenesis (El-Jaick et al., 2007).

In the mouse embryo, most fetal tissues derive from the epiblast, whereas the primitive endoderm, which initially covers the epiblast as visceral endoderm (VE) and then forms the yolk sac, is extra-embryonic (Arnold and Robertson, 2009). Extra-embryonic tissues provide signals that regulate formation of the basic body plan by initiating embryonic axis formation during gastrulation (Tam and Loebel, 2007; Tam et al., 2006). Anteroposterior (AP) axis specification begins when cells of the distal visceral endoderm (DVE) move toward the prospective anterior of the embryo to form the anterior visceral endoderm (AVE), breaking the radial symmetry of the embryo (Beddington and Robertson, 1999; Lu et al., 2001; Thomas and Beddington, 1996). Nodal is essential during gastrulation for mesoderm and endoderm formation from the primitive streak, and for AP and left-right (L-R) patterning (Brennan et al., 2001; Conlon et al., 1994). The extracellular Cerberus and Lefty antagonists interact

[1]Department of Biochemistry and Molecular Genetics, and Center for Cell Signaling and [2]Department of Cell Biology, University of Virginia, Box 800577, HSC, Charlottesville VA 22908, USA. [3]HHMI, Beth Israel Deaconess Medical Center, Harvard University, 330 Brookline Avenue Boston, MA 02215, USA.

*These authors contributed equally to this work
†Author for correspondence (dw2p@virginia.edu)

Accepted 16 November 2009

with Nodal or its co-receptors to block receptor activation by Nodal (Chen and Shen, 2004; Cheng et al., 2004; Piccolo et al., 1999). *Lefty* genes are also downstream targets of Nodal, forming a negative-feedback loop that regulates Nodal signaling (Branford and Yost, 2004; Meno et al., 1999). In the DVE, activation of Smad2 by Nodal induces characteristic patterns of gene expression that lead to the establishment of the AP axis of the embryo (Brennan et al., 2001; Mesnard et al., 2006; Waldrip et al., 1998). Nodal antagonists limit Nodal signaling in the anterior, while allowing higher levels of signaling in the posterior, leading to primitive streak formation. In the primitive streak, the epiblast cells undergo an epithelial-to-mesenchymal transition (EMT) to form mesoderm and definitive endoderm, thereby establishing the three primary germ layers (Arnold and Robertson, 2009; Tam and Loebel, 2007).

Loss of function of Nodal or of the intracellular mediators of Nodal signaling, Smad2 and Smad4, results in complete failure of gastrulation (Conlon et al., 1994; Sirard et al., 1998; Waldrip et al., 1998). The gastrulation failure with loss of *Smad2* can be rescued by the presence of wild-type extra-embryonic tissue (Waldrip et al., 1998). Similarly, *Smad4* mutations reveal a role for Smad4 in both the epiblast and extra-embryonic lineages during gastrulation (Chu et al., 2004; Sirard et al., 1998). Thus Nodal signaling through Smads is required both in extra-embryonic tissues and in the epiblast from the time of implantation through gastrulation for the formation of the embryonic axes that govern the body plan.

Here we demonstrate that loss-of-function mutations in both *Tgif1* and *Tgif2* in mice result in failure of gastrulation. Using a conditional allele of *Tgif1*, we show that Tgif1 is required in the extra-embryonic tissue for patterning the epiblast. Importantly, we show that reducing the dose of Nodal partially rescues these defects, providing the first evidence for an essential function of Tgifs in the Nodal pathway during mammalian embryogenesis.

MATERIALS AND METHODS

Tgif2 gene disruption and mice

The *Tgif1* null and the loxP flanked *Tgif1* alleles have been described previously (Bartholin et al., 2006; Shen and Walsh, 2005). The *Nodal* mutant and *Sox2-Cre* lines are as described (Collignon et al., 1996; Hayashi et al., 2002). To make the *Tgif2* mutant allele, a 16 kb genomic fragment containing exon 2 of *Tgif2* was isolated from mouse 129Sv/Ev DNA, and an 11 kb *Spe*I to *Not*I sub-fragment was used to make the targeting vector. The 5′ end of a *GFP* gene cassette was inserted 8 bp upstream of the start codon in exon 2. At the 3′ end of the targeting vector, a *Neo* gene in reverse orientation was inserted 110 bp downstream of exon 2, such that the *GFP* reporter and the *Neo* cassette replaced the coding region of exon 2 and part of intron 2. 129Sv/Ev embryonic stem cells were targeted and positive clones verified by PCR and Southern blotting. Following introduction of targeted embryonic stem cells into C57BL/6J blastocysts, chimeras were crossed to C57BL/6J and the strain was maintained on a mixed C57BL/6J × 129Sv/J background. All procedures were approved by the Animal Care and Use Committee of the University of Virginia.

DNA and RNA analyses

Genomic DNA for genotype analysis was purified from ear punch [at postnatal day 21 (P21)] or yolk sac [8.5-10.5 days post-coitum (dpc)] by HotShot (Truett et al., 2000) or from whole embryo by proteinase K digestion following in situ hybridization. Genotype was determined by PCR (see Table S1 in the supplementary material for primer sequences). DNA for Southern blotting was purified from adult liver by standard proteinase K digestion and phenol-chloroform extraction methods. Southern blotting was carried out using standard techniques. RNA was isolated and purified using the Absolutely RNA Miniprep Kit (Stratagene). For qRT-PCR, cDNA was generated using SuperScript III (Invitrogen) and analyzed in triplicate by real-time PCR using a Bio-Rad MyIQ cycler and SensiMix*Plus* SYBR plus FITC mix (Quantace), with intron spanning primer pairs (see Table S1 in the supplementary material), selected using Primer3 (http://frodo.wi.mit.edu/). Expression was normalized to Rpl4 using the delta Ct method, and is shown as mean plus standard deviation of triplicates.

Histology and whole-mount analyses

Implantation sites were fixed in 4% paraformaldehyde then embedded in paraffin. Sections 5 μm thick were de-paraffinized with SafeClear (Fisher) and stained with Hematoxylin and Eosin (H&E). Two to four sections each from at least three control and double null implantation sites were incubated with primary rabbit antibodies to Laminin (1:200, EY Labs), E-cadherin (1:25, Cell Signaling) or histone H3S10p (1:2000, Upstate), or mouse antibodies to N-cadherin (1:50, DSHB) or Foxa2 (1:50, DSHB), and secondary Alexa fluor 546-labeled goat anti-rabbit (1:2000, Invitrogen). For IHC, antibody staining was detected using Vectastain ABC (Vector Labs) and developed with Impact DAB (Vector Laboratories). Images were captured using an Olympus BX51 microscope and DP70 digital camera, and manipulated in Adobe Photoshop. Images of 6.5-10.5 dpc embryos were captured using a Leica MZ16 stereomicroscope and QImaging 5.0 RTV digital camera. For whole-mount immunofluorescence, 7.5 dpc embryos (four control and four double null) were fixed in 4% paraformaldehyde for 30 minutes, washed in PBS, permeabilized in 0.1% Triton X-100 for 2-5 minutes, then blocked in 10% FBS, 5% BSA in PBS for 1 hour, and incubated with goat anti-brachyury (1:50, SCBT) in PBS with 0.5% Tween 20 for 1 hour, followed by anti-goat Alexa fluor 488 (1:1000) for 30 minutes. After PBS-T washes and mounting on glass, dishes were analyzed by confocal microscopy.

In situ hybridization

Whole-mount in situ hybridization was performed on 6.5-8.5 dpc embryos per genotype with digoxigenin-labeled riboprobes, as described (Wilkinson, 1992). Images were captured as for unprocessed embryos. Stained embryos were processed for sectioning and histology as described (Sasaki and Hogan, 1993). All images are representative of at least three embryos analyzed, except where noted in the legends.

Luciferase assays

HepG2 cells were transfected using Exgen 500 (MBI Fermentas), with a Gsc luciferase reporter (Labbé et al., 1998), a Renilla transfection control (phCMVRLuc; Promega) and a Tgif1 expression construct. Activity was analyzed as previously described (Hyman et al., 2003).

RESULTS

Generation of a *Tgif2* mutant allele

We targeted the first coding exon of mouse *Tgif2*, which encodes the N-terminal 63 amino acids of Tgif2 (Fig. 1A). The coding sequence of this exon was replaced with sequences encoding eGFP, such that *eGFP* would be expressed from the *Tgif2* promoter. After verifying correct integration by PCR and Southern blotting (data not shown and Fig. 1B), we intercrossed *Tgif2* heterozygotes in a mixed C57BL/6J × 129Sv/J background. As with our *Tgif1* null allele, we found no significant deviation from the expected genotype frequencies in the offspring, and in this mixed strain background we have not identified any phenotypes of homozygous loss of *Tgif2* (see Table S2 in the supplementary material).

As the second coding exon was still present, we used qRT-PCR to test for expression of different regions of the *Tgif2* gene. We observed a decrease in *Tgif2* mRNA levels in the heterozygote when using one primer from each coding exon, and no signal was detected in the mutant (Fig. 1C). No expression was detected in the homozygous mutants using primers that span the *eGFP* sequence (primers A and Y, Fig. 1C), suggesting that the *eGFP* sequence was not being spliced to the downstream exon. As expected, an inverse pattern of mRNA expression was seen using primers that detect the integrated *GFP* allele (Fig. 1C). Analysis of expression of the remaining second coding exon (primers C and Z) revealed some

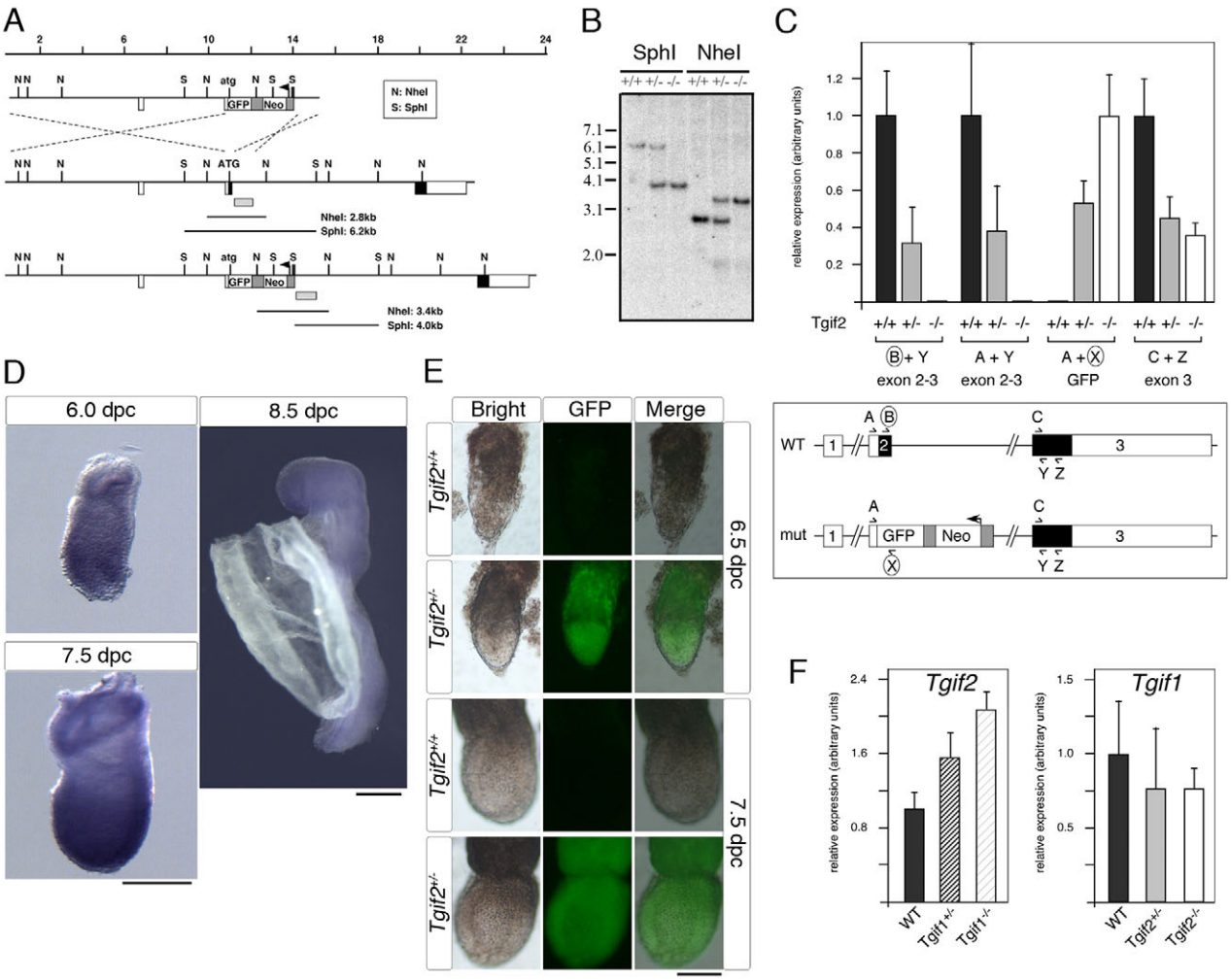

Fig. 1. Disruption of mouse *Tgif2*. (**A**) The targeting vector, *Tgif2* locus and targeted allele are shown, with restriction enzyme sites and predicted sizes of restriction fragments. Coding exons are shown in black. The gray bar indicates the probe used for Southern blotting. A scale bar (in kb) is shown above. (**B**) Genomic DNA of the indicated genotypes was subjected to restriction enzyme digestion and Southern blotting. (**C**) Expression of *Tgif2* mRNA was analyzed by qRT-PCR. Circles around primers B and X indicate that they anneal to sequences present only in the wild-type or targeted allele. Relative expression, normalized to Rpl4 is shown for the primer pairs indicated below. (**D**) Expression of *Tgif2* was analyzed by whole-mount in situ hybridization, in at least five embryos at each of the indicated ages. (**E**) Expression of the targeted allele was examined by observing eGFP fluorescence in three embryos of the indicated ages and genotypes. Fluorescent, brightfield and merged images are shown. (**F**) Expression of *Tgif2* and *Tgif1* was analyzed by qRT-PCR in 7.5 dpc littermates from *Tgif1* and *Tgif2* heterozygous intercrosses. Scale bars: in D, 250 μm (6.0-7.5 dpc) and 1 mm (8.5 dpc); 200 μm in E.

residual expression in the mutant. However, we have been unable to demonstrate that this region of the *Tgif2* gene encodes a stable functional protein, suggesting that this allele is likely to be a null.

We next analyzed expression of *Tgif2* from 6.0 to 8.5 dpc by in situ hybridization (ISH). We observed expression of *Tgif2* throughout the embryo proper at 6.0 and 7.5 dpc, with lower expression in the extra-embryonic ectoderm and endoderm (Fig. 1D). At 8.5 dpc, *Tgif2* expression was again seen throughout the embryo, but not in the yolk sac. We also analyzed expression of the *eGFP* allele in heterozygous embryos at 6.5 and 7.5 dpc by fluorescence. The targeted eGFP was widely expressed throughout the embryo and extra-embryonic ectoderm at both stages, but we observed no GFP signal in either the wild-type maternal tissue, or in wild-type littermate controls (Fig. 1E). To test whether there was any effect of deleting *Tgif1* on expression of *Tgif2*, we analyzed embryos from *Tgif1* heterozygous intercrosses for expression of *Tgif2* by ISH. Analysis of multiple litters did not reveal any consistent change in expression of *Tgif2* in embryos lacking *Tgif1*, although we did observe a two-fold increase in *Tgif2* mRNA levels in *Tgif1* null 7.5 dpc embryos by qRT-PCR (Fig. 1F). Similar analyses for *Tgif1* expression in the absence of *Tgif2* did not reveal any changes in expression, even by qRT-PCR. Thus, it appears that *Tgif2*, like *Tgif1*, is expressed throughout the early embryo, and that there is not a dramatic change in expression of either gene in the absence of the other.

Tgif1;Tgif2 double null embryos are unviable

We next generated *Tgif1*;*Tgif2* double heterozygotes, which were normal and fertile. Out of more than 300 weaned offspring from double heterozygote intercrosses, and an additional 112 from crosses between double heterozygous females and $Tgif1^{-/-};Tgif2^{+/-}$ males, none were double homozygous mutants (see Table S2 in the supplementary material). All other genotypes were found to be viable in this background, suggesting that a single wild-type allele of either gene can support normal development. However, mice with

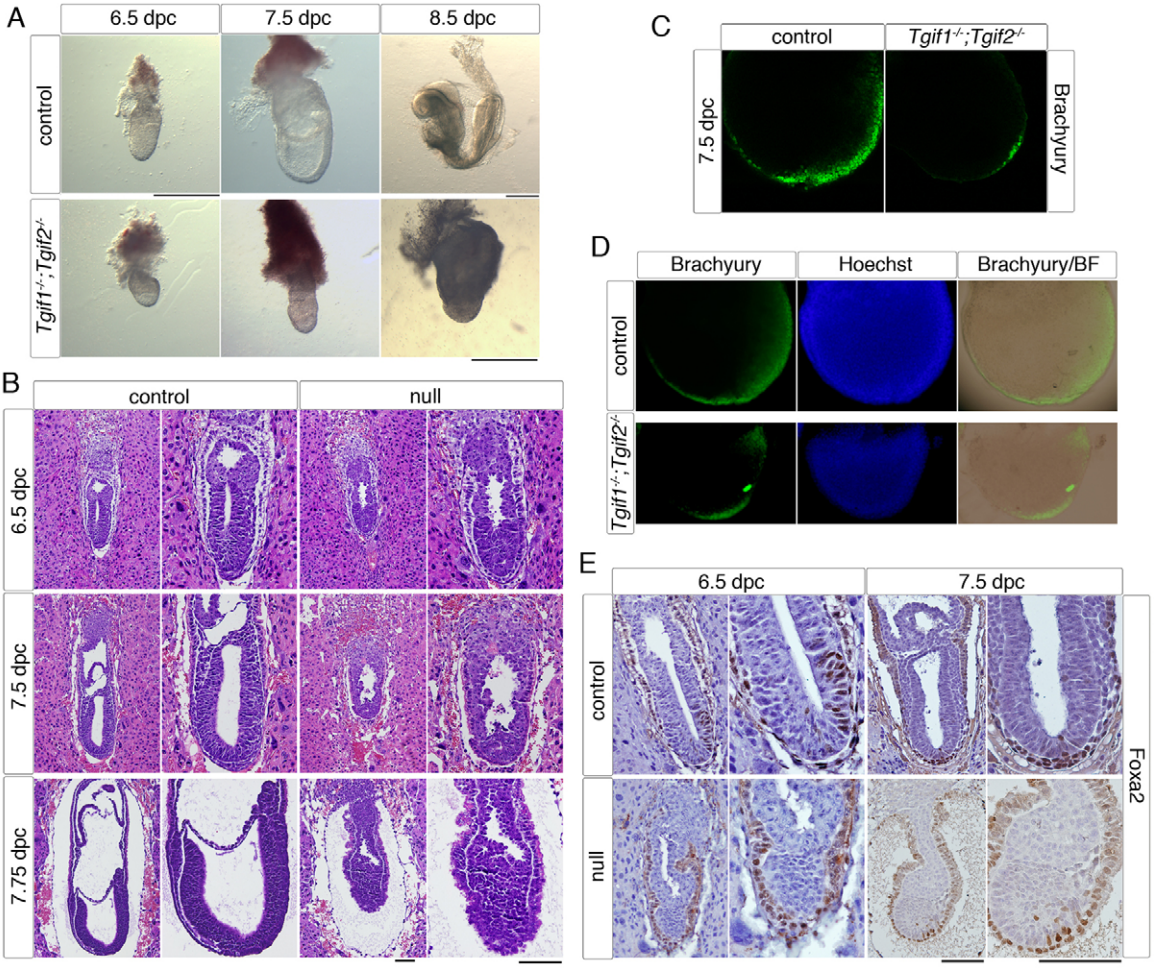

Fig. 2. *Tgif1*;*Tgif2* double null embryos fail to gastrulate. (**A**) Whole-mount images of embryos at the indicated ages, from *Tgif1*;*Tgif2* double mutant intercrosses and littermate controls. The genotype of the control embryos is not indicated, as they are representative of normal embryos from these crosses. (**B**) Hematoxylin and Eosin (H&E) stained sections of fixed and paraffin-embedded implantation sites at 6.5-7.75 dpc from *Tgif1*;*Tgif2* double mutant intercrosses; nulls and littermate controls are shown. (**C**) Control and double null embryos at 7.5 dpc were examined by indirect whole-mount immunofluorescence with a brachyury-specific antibody (green). A single *z* slice is shown, taken at 20× magnification by confocal microscopy. (**D**) Whole-mount images of control and double null embryos stained with a brachyury-specific antibody are shown, together with Hoechst stain for DNA, and an overlay of the brightfield and brachyury image. (**E**) Implantation sites at the indicated ages were analyzed with a Foxa2-specific antibody. Individual central sections are shown. Scale bars: 500 μm in A; 100 μm in B,E.

a total of three mutant alleles often showed reduced fertility and tended to be smaller than their littermates. We were able to isolate double homozygous mutant embryos from double heterozygous intercrosses at 7.5 and 8.5 dpc (9 out of 230 embryos at these two ages; see Table S2 in the supplementary material), but were unable to conclusively identify any double null embryos at 9.5 dpc or later, suggesting that *Tgif1*;*Tgif2* double null embryos do not survive beyond 8.5 dpc.

All of the double null embryos identified at 7.5 and 8.5 dpc were clearly defective; they were significantly smaller, and we were unable to identify a clear AP axis, even at 8.5 dpc (Fig. 2A). Comparison of double null embryos with littermate controls at 6.5 dpc revealed that at this stage they were more similar in size and shape, but with a rounder appearance of the embryo, suggesting decreased elongation of the proximodistal (PD) axis (Fig. 2A). We also found that a small proportion (less than 10%) of embryos with only a single wild-type allele at either *Tgif1* or *Tgif2* were indistinguishable from double nulls at 6.5 to 8.5 dpc, although the majority were normal at these stages. H&E staining of sectioned implantation sites from double mutant intercrosses showed that at 6.5 dpc defective embryos were of similar size to littermate controls, but cells within the epiblast were less well organized (Fig. 2B). By 7.5 dpc and later the lack of organization was even more apparent, such that cells of the epiblast failed to display the characteristic columnar epithelial morphology, and the embryo had not formed a distinct embryonic cavity. In some cases, the epiblast appeared to be a mass of disorganized cells with a more mesenchymal appearance (Fig. 2B). It also appeared that the formation or morphogenesis of the germ layers was impaired in the defective embryos, suggesting defects in gastrulation.

It was not possible to reliably determine whether the double nulls had formed an AP axis from the morphology evident in either whole-mount views or sections. To address this question we examined expression of the primitive streak marker, brachyury, by whole-mount immunofluorescence at 7.5 dpc. Robust staining of the primitive streak in the posterior was visible in control embryos at this stage (Fig. 2C,D). Interestingly, we did detect some staining in double null embryos, where it appeared to be localized to one side

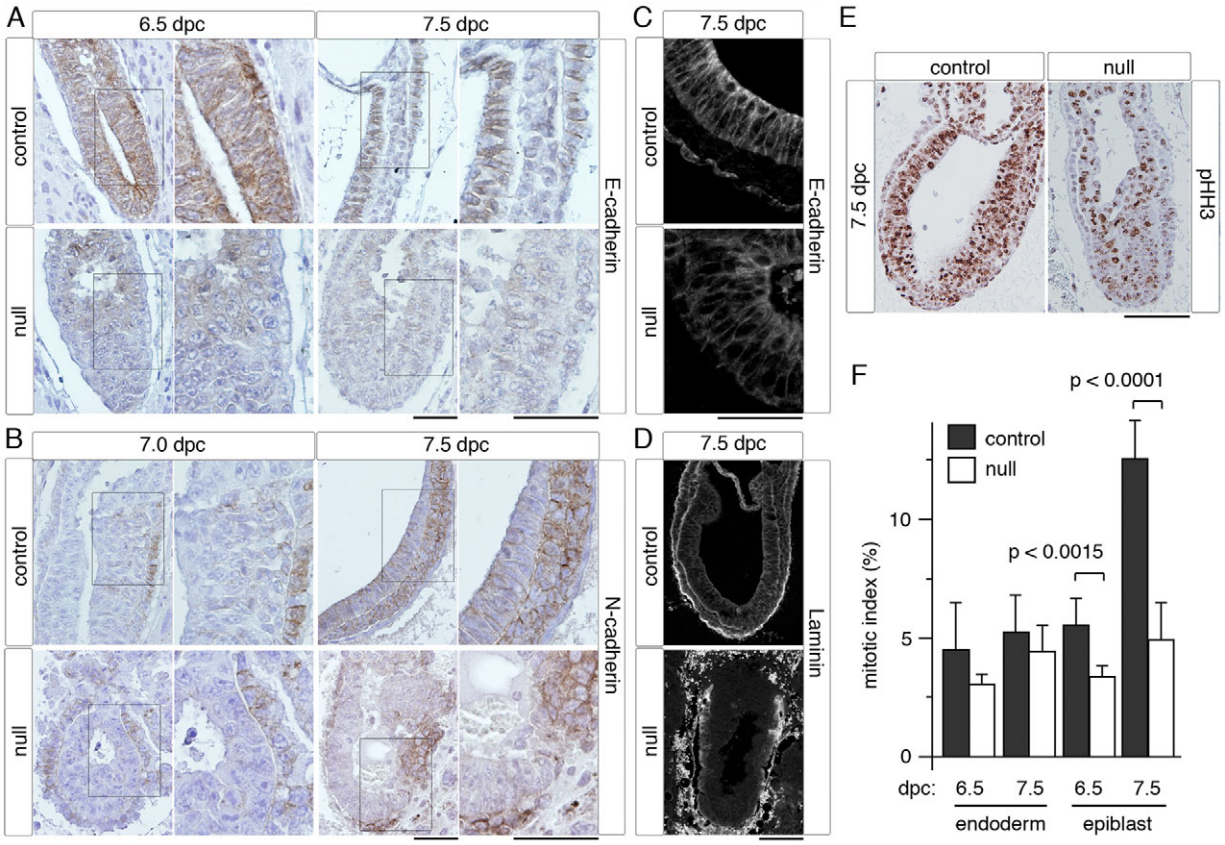

Fig. 3. Reduced epithelialization of *Tgif1*;*Tgif2* double null embryos. (**A**,**B**) Implantation sites at the indicated ages were analyzed by immunohistochemistry with antibodies for E-cadherin (A) or N-cadherin (B). The boxes indicate the regions shown at higher resolution to the right. (**C**,**D**) Implantation sites were analyzed by indirect immunofluorescence with an E-cadherin-specific antibody (C), or an antibody which recognizes laminin (D). (**E**) Implantation sites were analyzed by immunohistochemistry using an antibody for pHH3. Positively stained nuclei are a uniform dark brown. (**F**) Mitotic index within the endoderm and epiblast for each section was calculated as the percentage of pHH3-stained nuclei, for control and phenotypic double null embryos. Average ± s.d. of multiple sections is shown, with the significance level as calculated by Student's *t*-test. Scale bars: 100 μm in A,B,D,E; 50 μm in C.

of the embryo. Immunohistochemical analysis of embryo sections at 6.5-7.5 dpc revealed that expression of Foxa2 was considerably reduced in the mutants (Fig. 2E). At 6.5 dpc, nuclear Foxa2 staining was detected in the visceral endoderm and anterior primitive streak, but in the null was seen only in the visceral endoderm, with only a few positive cells present in the epiblast by 7.5 dpc. The reduced, but localized, brachyury expression combined with decreased Foxa2 staining suggests that the AP axis had been specified, and the primitive streak had been induced, but failed to elongate.

Decreased epithelialization of the epiblast

To examine cellular morphology in the epiblast more thoroughly, we stained sections with antibodies specific for either E-cadherin (cadherin 1 – Mouse Genome Informatics) or N-cadherin (cadherin 2). As shown in Fig. 3A, we observed a robust E-cadherin signal in the normal 6.5 dpc embryos, with the signal primarily localized to the edges of the cells. By contrast, there was relatively little E-cadherin expression in the defective embryos. By 7.5 dpc, E-cadherin staining was limited to the ectoderm and definitive endoderm in normal embryos, whereas in the defective embryos, there was a lower level of staining throughout the embryo that was not localized to the cell surface (Fig. 3A). At 7.0 dpc there was relatively little N-cadherin staining in the primitive streak of control embryos, but by 7.5 dpc robust staining was observed in the mesoderm (Fig. 3B). Despite the lower E-cadherin expression, we did not see increased expression of N-cadherin in the double nulls compared with control embryos, suggesting that there is a lack of epithelial morphology, without a transition to mesodermal fate.

In control embryos three germ layers are clearly evident, with distinct morphologies and different levels of E-cadherin staining. By contrast, defective embryos have not formed three distinct germ layers; rather there is an endodermal layer surrounding a disorganized mass of cells (Fig. 3C). Immunofluorescent staining with a laminin-specific antibody clearly identifies the basement membrane separating anterior ectoderm from mesendoderm in the normal embryos, which is absent in the double null, consistent with the lack of both polarization and epithelial morphology in epiblast cells (Fig. 3D). Together, these data suggest that embryos that completely lack Tgif1 and Tgif2 have defects in germ-layer formation.

Reduced proliferation in embryos lacking Tgif1 and Tgif2

To determine whether the smaller size of the double null embryos was a result of decreased proliferation rates, we stained multiple sections of control and double null embryos at 6.5 and 7.5 dpc with an antibody to histone H3, phosphorylated on serine 10 (pHH3), which is a marker of mitotic cells. Mitotic cells were seen throughout the control and defective embryos at 6.5 and 7.5 dpc (Fig. 3E and data not shown). As

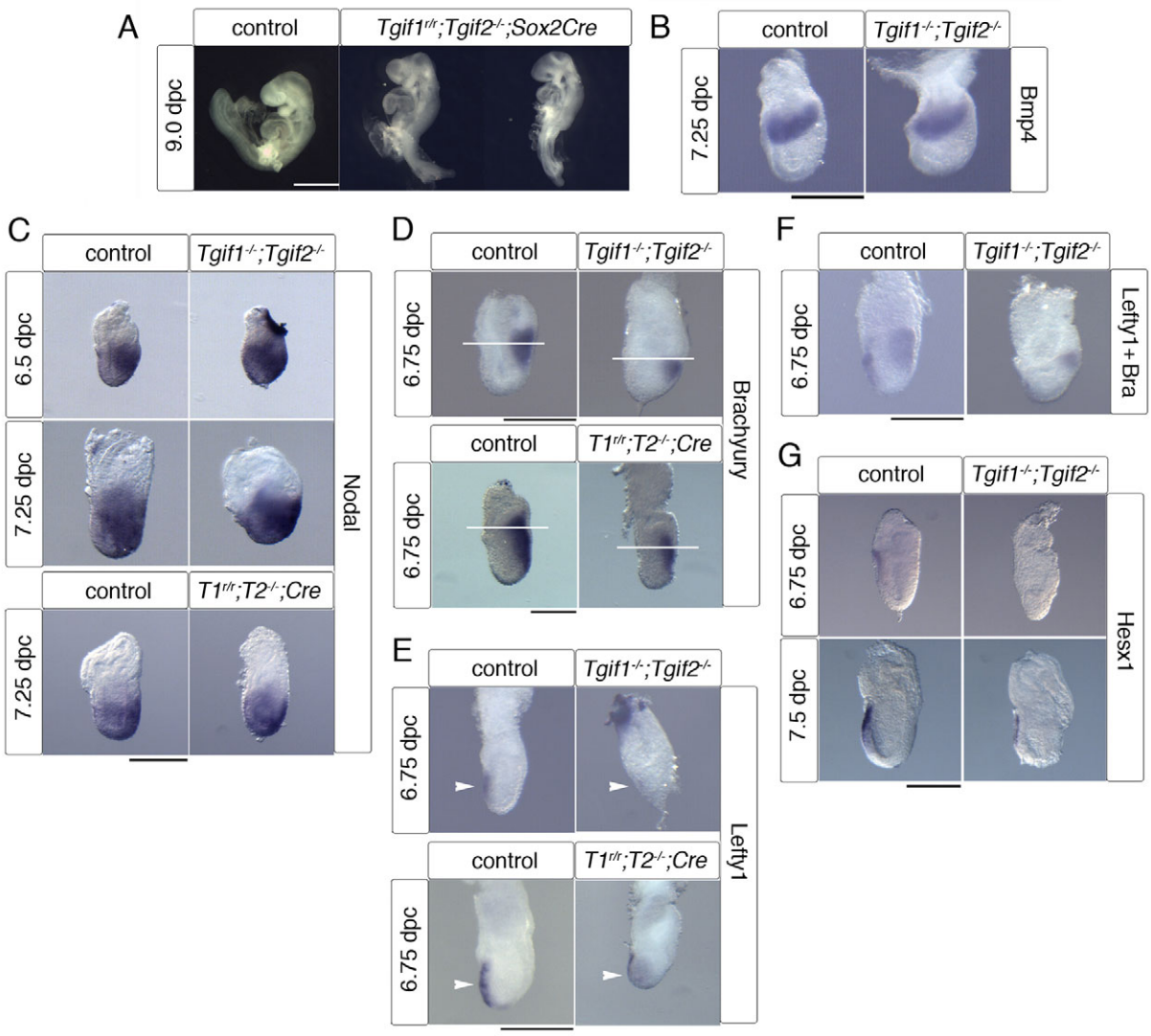

Fig. 4. Marker analysis in double null embryos. (**A**) Embryos at 9.0 dpc from *Tgif1*;*Tgif2* conditional double intercrosses with epiblast-specific deletion of the conditional *Tgif1* allele. (**B-G**) Embryos of the indicated genotypes, together with a littermate control, were analyzed by in situ hybridization for *Bmp4* (B), Nodal (C), brachyury (D), *Lefty1* (E), brachyury and *Lefty1* together (F) and *Hesx1* (G). In D, the white lines indicate the boundary between embryonic and extra-embryonic tissue. The arrowheads in E indicate the expected center of *Lefty1* staining. For panel C at 6.5 dpc and panels F and G, images of mutant embryos are representative of two embryos per stage. For panel E, the conditional double mutant is representative of five embryos. All other images are representative of three embryos for mutants, and at least five controls. Scale bars: 1 mm in A; 250 μm in B-G.

we could not distinguish ectoderm from mesoderm in defective embryos, we quantified pHH3 separately in the endoderm and epiblast. At 6.5 dpc the proliferation rates in visceral endoderm were not different between normal and defective embryos, whereas in the epiblast there was a lower proliferation rate in the defective embryos (Fig. 3F). By 7.5 dpc the difference in proliferation rates in the epiblast was even greater. We detected no consistent changes in rates of apoptosis between control and defective embryos (data not shown), suggesting that the size difference is primarily due to decreased proliferation in the absence of Tgif1 and Tgif2.

A requirement for Tgif1 in the extra-embryonic tissue

To determine whether there are separate requirements for Tgif1 in the embryonic and extra-embryonic tissues, we generated epiblast-specific double null embryos, using a conditional allele of *Tgif1* [Shen and Walsh referred to here as $Tgif1^{f}$, or $Tgif1^{r}$, when recombined (Shen and Walsh, 2005)] in combination with the *Tgif2* mutation and a *Sox2-Cre* transgene (Hayashi et al., 2002). We crossed $Tgif1^{f/f};Tgif2^{-/-}$ females with either $Tgif1^{+/r};Tgif2^{+/-};Sox2Cre^{+}$ or $Tgif1^{r/r};Tgif2^{+/-};Sox2Cre^{+}$ males and analyzed the genotypes of offspring at P21. Among 150 offspring from these crosses we never observed any double null mice, suggesting that Tgif function is required in the epiblast (see Table S3 in the supplementary material). We observed double null embryos in these crosses at 7.5 and 8.5 dpc at close to the expected frequency. However, unlike the constitutive double null, epiblast-specific double null embryos had clearly undergone gastrulation and formed distinct anterior neural structures. Additionally, the conditional double nulls were present up to 10.5 dpc (Fig. 4A and Table S3 in the supplementary material). At 9.5-10.5 dpc these embryos had an elongated AP axis; in many cases they had at least

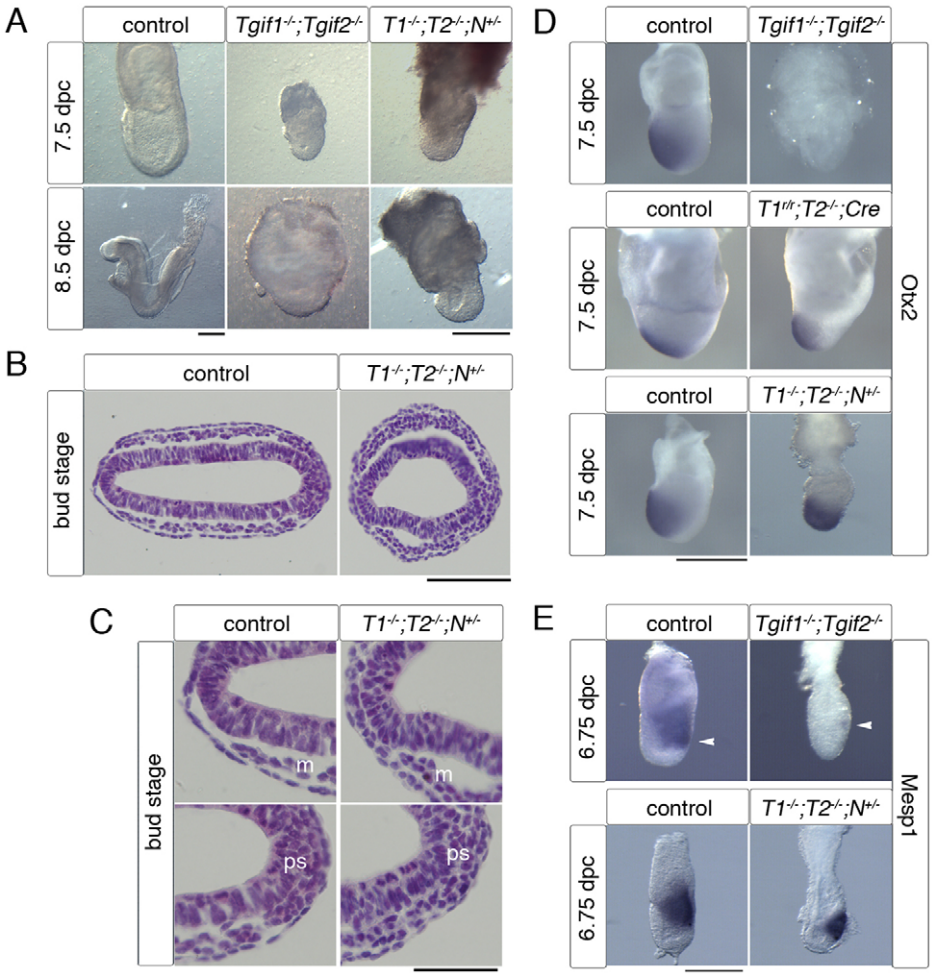

Fig. 5. Analysis of Tgif function in the Nodal pathway. (**A**) Whole-mount images of control embryos and 7.5-8.5 dpc *Tgif1*;*Tgif2* double null embryos, with or without a heterozygous mutation in the *Nodal* gene. (**B**) H&E stained transverse sections through late alantoic bud stage embryos, with anterior to the left. (**C**) Higher resolution images of the sections in B. Images were captured at 20× (B) or 40× (C) magnification. (**D**,**E**) *Otx2* (D) and *Mesp1* (E) expression was analyzed by in situ hybridization in embryos of the indicated genotypes. For panel E, two *Tgif1*$^{-/-}$;*Tgif2*$^{-/-}$;*Nodal*$^{+/-}$ embryos were analyzed. All other images are representative of at least three mutant or five control embryos. Scale bars: 250 μm in A,D,E; 100 μm in B; 50 μm in C. m, mesoderm; ps, primitive streak.

begun to turn, and had initiated organogenesis. However, they were clearly delayed and had other developmental defects, including defects in anterior structures, heart and somites. Importantly, this result suggests that Tgif1 present in the extra-embryonic tissue plays a crucial role in directing the development of the epiblast.

Analysis by ISH showed that *Bmp4*, which is normally expressed in the extra-embryonic ectoderm, and regulates mesoderm induction, was not different between control and double null embryos (Fig. 4B). Similarly, *Nodal* expression was seen in both constitutive and conditional double null embryos, and did not appear to be significantly different from controls (Fig. 4C). Expression of brachyury in both constitutive and epiblast-specific double null embryos was reduced compared to control embryos (Fig. 4D), consistent with the immunofluorescent analysis (Fig. 2). The Nodal antagonist, Lefty1, is normally expressed in the AVE, and modulates Nodal signaling in the epiblast. *Lefty1* expression was clearly reduced in the constitutive double null at 6.75 dpc, although expression was restricted to what is presumably the anterior of the embryo (Fig. 4E). In the epiblast-specific double nulls, the area of *Lefty1* signal appears to be increased relative to the constitutive double null, supporting a role for Tgif in the extra-embryonic endoderm. To test whether the regionalized expression of *Lefty1* and brachyury in the constitutive double null embryos was consistent with the presence of an AP axis, we stained embryos with both probes together, and observed expression of *Lefty1* and brachyury on opposite sides of the double null embryo (Fig. 4F). *Hesx1* expression was observed in the AVE from 6.75 dpc and in the prospective anterior of the embryo by 7.5 dpc, whereas its expression was clearly reduced in embryos lacking all Tgif function (Fig. 4G). It appears that in the complete absence of all Tgif function AP axis specification still occurs but the primitive streak fails to elongate, and the reduced *Lefty1* and *Hesx1* expression suggests that AVE morphogenesis is impaired.

A role for Tgifs in the Nodal pathway

To test whether any of the phenotypes observed in the double null embryos was due to de-repression of the Nodal pathway, we introduced a heterozygous *Nodal* mutation into our constitutive double nulls. Initial observation of 7.5-8.5 dpc embryos suggested some rescue of the double null phenotype (Fig. 5A): the *Tgif1*;*Tgif2* double mutants with a heterozygous *Nodal* mutation had formed an embryonic cavity at 8.5 dpc, rather than the disorganized ball of cells seen in the double null. To better characterize the morphology of Nodal rescue embryos, we H&E-stained transverse sections through the embryonic cavity of stage-matched late allantoic bud stage control and *Tgif1*;*Tgif2* double nulls with a *Nodal* heterozygous mutation. The double nulls with a *Nodal* heterozygous mutation had formed a distinct cavity and had generated three germ layers, with mesoderm clearly present (Fig. 5B,C), rather than the disorganized ball of cells seen in the double null (see Fig. 2 for comparison). Additionally, it was possible to distinguish an AP axis in these embryos, suggesting a significant rescue of the double null phenotype. We next analyzed double nulls with *Nodal* heterozygous mutations by ISH.

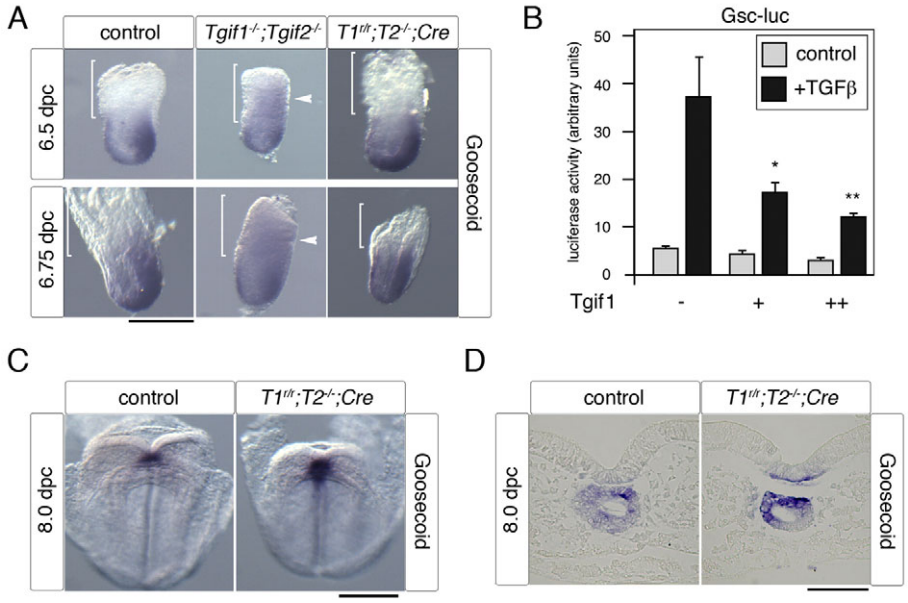

Fig. 6. Regulation of goosecoid expression by Tgifs. (**A**) Embryos of the indicated ages and genotypes were analyzed for expression of goosecoid by in situ hybridization. The brackets indicate the extra-embryonic region. Arrowheads indicate expression in the extra-embryonic region. (**B**) A goosecoid promoter reporter construct was used to test repression by co-expressed Tgif1 (+, 20 ng/well, ++, 50 ng/well) in transfected HepG2 cells. Cells were treated with TGFβ, as indicated. Results are presented as means±s.d. of triplicate transfections, normalized to a Renilla luciferase control. Activity in the presence of Tgif1 was significantly different from the control (*P<0.05, **P<0.01), as determined by Student's t-test. (**C**) Expression of goosecoid in 8.0 dpc embryos of the indicated genotypes was analyzed by in situ hybridization. (**D**) Sections through the embryos in C. All in situ images are representative of at least three embryos. Scale bars: 250 μm in A,C; 100 μm in D.

Strikingly, *Otx2*, a marker of anterior presumptive neuroectoderm, was not expressed in the constitutive double null embryos, but its expression was clearly restored either by a *Nodal* heterozygous mutation, or by the presence of a single wild-type allele of *Tgif1* in the extra-embryonic tissue (Fig. 5D). We observed little expression of the mesodermal marker, *Mesp1*, in double null embryos at 6.75 dpc, whereas, in double nulls with a *Nodal* heterozygous mutation, *Mesp1* expression was significantly restored (Fig. 5E). Together, these results strongly suggest that during gastrulation, Tgif function is required to limit Nodal signaling.

Goosecoid homeobox (*Gsc*) is a direct target for activation by Smad complexes in response to Nodal (Labbé et al., 1998). We therefore decided to analyze its expression in embryos lacking Tgif function. As shown in Fig. 6A, *Gsc* expression is highest in the AVE and the primitive streak, but is absent from extra-embryonic tissue other than the AVE. In the double null embryos, we observed an expansion of the expression domain of *Gsc*, most strikingly into the extra-embryonic region. By contrast, apart from the AVE expression, *Gsc* is clearly absent from the extra-embryonic tissue in the epiblast-specific double null embryos, consistent with a direct role for Tgif1 as a repressor of *Gsc* expression. To confirm that Tgif1 could affect *Gsc* promoter activity, we analyzed a Gsc-luciferase reporter in transfected cells. This reporter was activated by addition of TGFβ, and its activity was clearly repressed by co-expression of increasing amounts of Tgif1 (Fig. 6B). To gain further in vivo evidence for regulation of *Gsc* by Tgifs, we examined its expression in the prechordal mesoderm at 8.0 dpc by ISH. We observed a clear increase in the intensity of the *Gsc* signal in the conditional double null embryos compared to controls, suggesting that at this stage of embryogenesis Tgifs repress *Gsc* expression (Fig. 6C,D). Together, these results suggest that Tgif function limits the transcriptional output of Nodal signaling.

Tgifs regulate L-R asymmetry

Nodal is a key regulator of the situs restricted expression of genes such as *Pitx2*, and is required for correct heart looping (Schier and Shen, 2000). To gain further evidence for a role for Tgif function in the Nodal pathway, we examined the formation of L-R asymmetry in epiblast-specific double null embryos. We found three distinct phenotypes with respect to heart looping in these embryos at 9.5 dpc (Fig. 7A): those in which looping had proceeded correctly (left to right), those with a reversal (right to left) and a third class in which the heart loop had extended dorsoventrally. In embryos with at least one wild-type allele of either *Tgif1* or *Tgif2* in the embryo, the heart looped correctly in every case examined (Fig. 7B). By contrast, among 17 epiblast-specific double null embryos we saw similar proportions of embryos with left-to-right and reversed heart looping. Additionally, in about a quarter of the embryos the heart tube extended without looping to either side. *Pitx2*, which is downstream of *Nodal* and is normally expressed only on the left lateral plate mesoderm (LPM) at 8.5 dpc, was expressed bilaterally at this stage of development in all epiblast-specific double nulls examined (Fig. 7C). Bilateral expression of *Pitx2* was suppressed in epiblast-specific double null embryos carrying a *Nodal* heterozygous mutation, such that *Pitx2* was restricted to one side of the LPM (Fig. 7C). However, even though *Pitx2* was expressed unilaterally in these Nodal rescue embryos, its expression was not always restricted to the left LPM as in a wild-type embryo. Thus, it appears that reducing the dose of Nodal can compensate to some degree for loss of Tgif function with regard to L-R asymmetry. Taken together with the effect of the *Nodal* heterozygous mutation on the phenotypes in constitutive double null embryos, these data clearly suggest that Tgif function is required to limit Nodal signaling during embryogenesis, and that Tgifs play a key role both in gastrulation and later during L-R patterning.

DISCUSSION

Tgif1 and Tgif2 are Smad transcriptional co-repressors, and we demonstrate here that Tgif function is essential for gastrulation in mice. Furthermore, we provide evidence that Tgifs function in the Nodal pathway, and that Tgif1 in the extra-embryonic tissue plays a crucial role in patterning the epiblast during gastrulation.

Previous studies of *Tgif1* null mice found no severe phenotypes in a mixed strain background, raising questions as to the role of Tgif1 during mouse development (Bartholin et al., 2006; Jin et al., 2006; Mar and Hoodless, 2006; Shen and Walsh, 2005). One obvious candidate for a compensatory factor is Tgif2, which

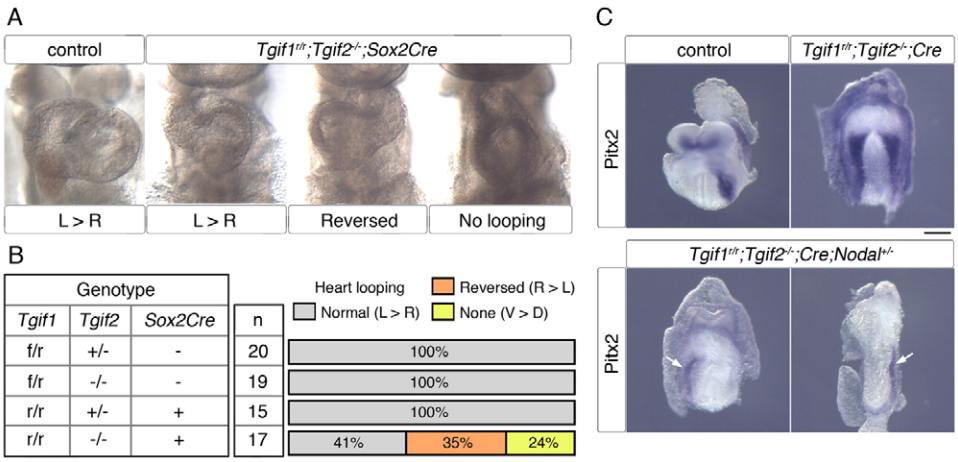

Fig. 7. Regulation of left-right asymmetry by Tgifs. (**A**) Whole-mount 9.5 dpc embryos of the indicated genotypes. Images were taken ventrally, such that the left of the embryo is to the right. (**B**) A summary of heart looping data from 9.5 dpc embryos from conditional double mutant intercrosses. Total numbers of embryos of each genotype and the percentage with each phenotype are shown. (**C**) Expression of *Pitx2* was analyzed by in situ hybridization at 8.5 dpc in embryos of the indicated genotypes: five conditional double mutant and three with the *Nodal* mutation. Two embryos are shown for the conditional double mutant with a heterozygous *Nodal* mutation, as two phenotypes were observed. Arrows indicate unilateral *Pitx2* expression in the *Nodal* heterozygotes. Scale bar: 250 μm.

shares considerable homology with Tgif1. Tgif2 interacts with the mSin3/HDAC complex to repress transcription, and can interact with TGFβ-activated Smads, suggesting conserved function (Melhuish et al., 2001; Melhuish and Wotton, 2006). *Tgif1* is expressed at high levels throughout the epiblast from 6.0 dpc, and at a lower level in extra-embryonic endoderm and ectoderm (Jin et al., 2006). *Tgif2* is expressed throughout the embryo and extra-embryonic tissue from 6.0 dpc onwards, consistent with the possibility of overlapping function. We show that homozygous mutation of mouse *Tgif2* does not cause appreciable phenotypes in a mixed strain background, similar to the *Tgif1* null. Mice with both *Tgif1* and *Tgif2* mutations are viable in this background, providing there is at least one wild-type allele of either *Tgif1* or *Tgif2*. By contrast, homozygous loss-of-function mutations at both loci results in a failure of gastrulation, suggesting that Tgif1 and Tgif2 perform essential overlapping functions during gastrulation.

Complete loss of Tgif function causes a growth delay, decreased epithelial morphology and disorganization of cells within the epiblast, and a failure to form three distinct germ layers. These defects are characteristic of failed gastrulation, and have some similarities to phenotypes seen with mutations in components of the Nodal pathway. In *Tgif1*;*Tgif2* double null embryos E-cadherin expression is decreased, and the protein appears not to be present at the cell surface. Additionally, the cells of the epiblast do not have the characteristic columnar epithelial morphology, and appear to be more mesenchymal in nature. However, there is no increase in N-cadherin expression and no increase in expression of mesodermal markers, such as *Mesp1* or brachyury. Thus, this appears to be a failure of epithelialization rather than true EMT. Despite the lack of obvious morphological landmarks, embryos lacking Tgif1 and Tgif2 establish the AP axis, as shown by expression of *Lefty1* and brachyury at opposite sides of the embryo. The primitive streak, as marked by brachyury expression, is induced but fails to extend, a defect which may in part be due to the developmental delay or decreased proliferation in these embryos. Expression of *Lefty1* is normally seen in the AVE, and in embryos lacking both Tgifs expression of *Lefty1* is reduced, and these cells have not migrated fully to the anterior. Together these data suggest that Tgif function is dispensable until after AP axis formation but is absolutely required for gastrulation to proceed normally.

An in vivo demonstration of a role for Tgif1 or Tgif2 function in the Nodal/TGFβ pathway has so far remained elusive. However, we show that a *Nodal* heterozygous mutation partially rescues the gastrulation defect seen in *Tgif1*;*Tgif2* double mutants, such that three germ layers are formed by the late allantoic bud stage. Additionally, *Nodal* heterozygosity restores expression of both the anterior neuroectoderm marker, *Otx2*, and the mesodermal marker, *Mesp1*, expression of which is severely decreased in double null embryos. Furthermore, analysis of the conditional double mutants shows that L-R patterning defects are also suppressed to some degree by *Nodal* heterozygosity. These observations clearly support a role for Tgif1 and Tgif2 in the regulation of Nodal signaling during development, although we cannot rule out the possibility that the initial defects in AVE morphogenesis may be Nodal independent. However, as Tgifs are transcriptional co-repressors for TGFβ-activated Smads, the simplest model is that Tgifs function to limit the transcriptional output via Smad2, in response to Nodal signals. Consistent with this, we show that expression of the Nodal/Smad2 target gene, *Gsc*, is increased in both the constitutive and conditional double mutants. Additionally, in transfected cells, Tgif1 repressed a *Gsc* promoter reporter, suggesting direct regulation of this Smad target gene by Tgif1.

A primary function of the Tgifs during gastrulation may be to regulate morphogenesis of the AVE, which in turn patterns the epiblast. The Nodal antagonists Cerberus-like (Cerl) and Lefty1 are expressed in the AVE, and regulate Nodal signaling in the epiblast. Although *Cerl*;*Lefty1* compound mutants have primitive streak defects that can be rescued by *Nodal* heterozygosity, they differ from our mutants, perhaps because of the restricted expression pattern of *Cerl* and *Lefty1*, compared with the more widespread expression of *Tgif1* and *Tgif2* (Perea-Gomez et al., 2002). At 5.5 dpc, Nodal in the epiblast positively regulates its own expression but is also subject to inhibition by Cerl and Lefty1, released from the visceral endoderm. In the absence of all

Tgif function, Nodal signaling in the epiblast might be de-repressed as a result of the loss of direct repression, and the pathway may be further de-regulated by inadequate production of extracellular antagonists. Indeed, *Lefty1* expression in *Tgif1*;*Tgif2* double mutants is decreased, and it appears that the AVE has not fully migrated towards the anterior. Restoration of a wild-type allele of *Tgif1* in the extra-embryonic region allows for primitive streak elongation with relatively normal *Lefty1* expression, and these embryos gastrulate. Defects in the epiblast of double null embryos may result from a combination of defects in both the visceral endoderm and the epiblast itself, although it appears that inappropriate production of antagonists in the AVE may be the primary defect, as gastrulation occurs relatively normally in the conditional double nulls.

In summary, we suggest that a major function of Tgifs is to allow for gastrulation, and the correct morphogenesis of the AVE. Our data support the argument that defects in the epiblast are in large part secondary to defects in the AVE. Thus in the absence of all Tgif function, the AVE fails to form correctly, and does not produce appropriate levels of Nodal inhibitors such as Lefty1, thereby causing defects in epiblast patterning. However, we cannot rule out a contribution of more direct effects of Tgifs in the epiblast, and our analysis of L-R defects in the conditional double mutants clearly support a role for Tgifs in the embryo proper (albeit at a later stage). This work provides the first clear evidence for a role for Tgif function during mammalian embryogenesis, and demonstrates that Tgif1 and Tgif2 act to limit signaling by the Nodal pathway during gastrulation and L-R axis specification. Thus the Tgifs are key regulators of the developmental response to TGFβ family ligands.

Acknowledgements

We thank E. J. Robertson and M. Shen for the *Nodal* mutant, and E. J. Robertson, M. R. Kuehn, J. F. Martin, J. Yu and W. Shawlot for in situ probes, and W. Shawlot for critical comments. Foxa2 and N-cadherin antibodies were developed by T. M. Jessell, and M. Takeichi and H. Matsunami (NICHD Developmental Studies Hybridoma Bank, maintained by the University of Iowa, Department of Biological Sciences). We thank UVA Research Histology Core, and InGenious Targeting for construction of *Tgif2* null mice. This work was supported in part by research Grant 6-FY04-77 from the March of Dimes (D.W.), and by NIH grants to D.W. (HD52707) and to A.E.S. (HD034807). J.S. and C.A.W. are supported by HHMI. Deposited in PMC for release after 6 months.

Competing interests statement

The authors declare no competing financial interests

Supplementary material

Supplementary material for this article is available at http://dev.biologists.org/lookup/suppl/doi:10.1242/dev.040782/-/DC1

References

Arnold, S. J. and Robertson, E. J. (2009). Making a commitment: cell lineage allocation and axis patterning in the early mouse embryo. *Nat. Rev. Mol. Cell Biol.* **10**, 91-103.

Bartholin, L., Powers, S. E., Melhuish, T. A., Lasse, S., Weinstein, M. and Wotton, D. (2006). TGIF inhibits retinoid signaling. *Mol. Cell. Biol.* **26**, 990-1001.

Bartholin, L., Melhuish, T. A., Powers, S. E., Goddard-Leon, S., Treilleux, I., Sutherland, A. E. and Wotton, D. (2008). Maternal Tgif is required for vascularization of the embryonic placenta. *Dev. Biol.* **319**, 285-297.

Beddington, R. S. and Robertson, E. J. (1999). Axis development and early asymmetry in mammals. *Cell* **96**, 195-209.

Bertolino, E., Reimund, B., Wildt-Perinic, D. and Clerc, R. (1995). A novel homeobox protein which recognizes a TGT core and functionally interferes with a retinoid-responsive motif. *J. Biol. Chem.* **270**, 31178-31188.

Branford, W. W. and Yost, H. J. (2004). Nodal signaling: CrypticLefty mechanism of antagonism decoded. *Curr. Biol.* **14**, R341-R343.

Brennan, J., Lu, C. C., Norris, D. P., Rodriguez, T. A., Beddington, R. S. and Robertson, E. J. (2001). Nodal signalling in the epiblast patterns the early mouse embryo. *Nature* **411**, 965-969.

Chen, C. and Shen, M. M. (2004). Two modes by which Lefty proteins inhibit nodal signaling. *Curr. Biol.* **14**, 618-624.

Cheng, S. K., Olale, F., Brivanlou, A. H. and Schier, A. F. (2004). Lefty blocks a subset of TGFbeta signals by antagonizing EGF-CFC coreceptors. *PLoS Biol.* **2**, E30.

Chu, G. C., Dunn, N. R., Anderson, D. C., Oxburgh, L. and Robertson, E. J. (2004). Differential requirements for Smad4 in TGFbeta-dependent patterning of the early mouse embryo. *Development* **131**, 3501-3512.

Collignon, J., Varlet, I. and Robertson, E. J. (1996). Relationship between asymmetric nodal expression and the direction of embryonic turning. *Nature* **381**, 155-158.

Conlon, F. L., Lyons, K. M., Takaesu, N., Barth, K. S., Kispert, A., Herrmann, B. and Robertson, E. J. (1994). A primary requirement for nodal in the formation and maintenance of the primitive streak in the mouse. *Development* **120**, 1919-1928.

El-Jaick, K. B., Powers, S. E., Bartholin, L., Myers, K. R., Hahn, J., Orioli, I. M., Ouspenskaia, M., Lacbawan, F., Roessler, E., Wotton, D. et al. (2007). Functional analysis of mutations in TGIF associated with holoprosencephaly. *Mol. Genet. Metab.* **90**, 97-111.

Gripp, K. W., Wotton, D., Edwards, M. C., Roessler, E., Ades, L., Meinecke, P., Richieri-Costa, A., Zackai, E. H., Massague, J., Muenke, M. et al. (2000). Mutations in TGIF cause holoprosencephaly and link NODAL signalling to human neural axis determination. *Nat. Genet.* **25**, 205-208.

Hayashi, S., Lewis, P., Pevny, L. and McMahon, A. P. (2002). Efficient gene modulation in mouse epiblast using a Sox2Cre transgenic mouse strain. *Mech. Dev.* **119 Suppl. 1**, S97-S101.

Heldin, C.-H., Miyazono, K. and ten Dijke, P. (1997). TGF-β signalling from cell membrane to nucleus through SMAD proteins. *Nature* **390**, 465-471.

Hyman, C. A., Bartholin, L., Newfeld, S. J. and Wotton, D. (2003). Drosophila TGIF proteins are transcriptional activators. *Mol. Cell. Biol.* **23**, 9262-9274.

Imoto, I., Pimkhaokham, A., Watanabe, T., Saito-Ohara, F., Soeda, E. and Inazawa, J. (2000). Amplification and overexpression of TGIF2, a novel homeobox gene of the TALE superclass, in ovarian cancer cell lines. *Biochem. Biophys. Res. Commun.* **276**, 264-270.

Itoh, S. and ten Dijke, P. (2007). Negative regulation of TGF-beta receptor/Smad signal transduction. *Curr. Opin. Cell Biol.* **19**, 176-184.

Jin, J. Z., Gu, S., McKinney, P. and Ding, J. (2006). Expression and functional analysis of Tgif during mouse midline development. *Dev. Dyn.* **235**, 547-553.

Kuang, C., Xiao, Y., Yang, L., Chen, Q., Wang, Z., Conway, S. J. and Chen, Y. (2006). Intragenic deletion of Tgif causes defectsin brain development. *Hum. Mol. Genet.* **15**, 3508-3519.

Labbé, E., Silvestri, C., Hoodless, P. A., Wrana, J. L. and Attisano, L. (1998). Smad2 and Smad3 positively and negatively regulate TGFß-dependent transcription through the forkhead DNA-binding protein FAST2. *Mol. Cell* **2**, 109-120.

Lu, C. C., Brennan, J. and Robertson, E. J. (2001). From fertilization to gastrulation: axis formation in the mouse embryo. *Curr. Opin. Genet. Dev.* **11**, 384-392.

Mar, L. and Hoodless, P. A. (2006). Embryonic fibroblasts from mice lacking Tgif were defective in cell cycling. *Mol. Cell. Biol.* **26**, 4302-4310.

Massagué, J. (1998). TGFβ signal transduction. *Annu. Rev. Biochem.* **67**, 753-791.

Massagué, J., Seoane, J. and Wotton, D. (2005). Smad transcription factors. *Genes Dev.* **19**, 2783-2810.

Melhuish, T. A. and Wotton, D. (2000). The interaction of C-terminal binding protein with the Smad corepressor TG-interacting factor is disrupted by a holoprosencephaly mutation in TGIF. *J. Biol. Chem.* **275**, 39762-39766.

Melhuish, T. A. and Wotton, D. (2006). The Tgif2 gene contains a retained intron within the coding sequence. *BMC Mol. Biol.* **7**, 2.

Melhuish, T. A., Gallo, C. M. and Wotton, D. (2001). TGIF2 interacts with histone deacetylase 1 and represses transcription. *J. Biol. Chem.* **26**, 26.

Meno, C., Gritsman, K., Ohishi, S., Ohfuji, Y., Heckscher, E., Mochida, K., Shimono, A., Kondoh, H., Talbot, W. S., Robertson, E. J. et al. (1999). Mouse Lefty2 and zebrafish antivin are feedback inhibitors of nodal signaling during vertebrate gastrulation. *Mol. Cell* **4**, 287-298.

Mesnard, D., Guzman-Ayala, M. and Constam, D. B. (2006). Nodal specifies embryonic visceral endoderm and sustains pluripotent cells in the epiblast before overt axial patterning. *Development* **133**, 2497-2505.

Perea-Gomez, A., Vella, F. D., Shawlot, W., Oulad-Abdelghani, M., Chazaud, C., Meno, C., Pfister, V., Chen, L., Robertson, E., Hamada, H. et al. (2002). Nodal antagonists in the anterior visceral endoderm prevent the formation of multiple primitive streaks. *Dev. Cell* **3**, 745-756.

Piccolo, S., Agius, E., Leyns, L., Bhattacharyya, S., Grunz, H., Bouwmeester, T. and De Robertis, E. M. (1999). The head inducer Cerberus is a multifunctional antagonist of Nodal, BMP and Wnt signals. *Nature* **397**, 707-710.

Sasaki, H. and Hogan, B. L. (1993). Differential expression of multiple fork head related genes during gastrulation and axial pattern formation in the mouse embryo. *Development* **118**, 47-59.

Schier, A. F. and Shen, M. M. (2000). Nodal signalling in vertebrate development. *Nature* **403**, 385-389.

Sharma, M. and Sun, Z. (2001). 5′TG3′ interacting factor interacts with Sin3A and represses AR- mediated transcription. *Mol. Endocrinol.* **15**, 1918-1928.
Shen, J. and Walsh, C. A. (2005). Targeted disruption of Tgif, the mouse ortholog of a human holoprosencephaly gene, does not result in holoprosencephaly in mice. *Mol. Cell. Biol.* **25**, 3639-3647.
Sirard, C., de la Pompa, J. L., Elia, A., Itie, A., Mirtsos, C., Cheung, A., Hahn, S., Wakeman, A., Schwartz, L., Kern, S. E. et al. (1998). The tumor suppressor gene *Smad4/DPC4* is required for gastrulation and later for anterior development of the mouse embryo. *Genes Dev.* **12**, 107-119.
Tam, P. P. and Loebel, D. A. (2007). Gene function in mouse embryogenesis: get set for gastrulation. *Nat. Rev. Genet.* **8**, 368-381.
Tam, P. P., Loebel, D. A. and Tanaka, S. S. (2006). Building the mouse gastrula: signals, asymmetry and lineages. *Curr. Opin. Genet. Dev.* **16**, 419-425.
Thomas, P. and Beddington, R. (1996). Anterior primitive endoderm may be responsible for patterning the anterior neural plate in the mouse embryo. *Curr. Biol.* **6**, 1487-1496.
Truett, G. E., Heeger, P., Mynatt, R. L., Truett, A. A., Walker, J. A. and Warman, M. L. (2000). Preparation of PCR-quality mouse genomic DNA with hot sodium hydroxide and tris (HotSHOT). *Biotechniques* **29**, 52, 54.
Waldrip, W. R., Bikoff, E. K., Hoodless, P. A., Wrana, J. L. and Robertson, E. J. (1998). Smad2 signaling in extraembryonic tissues determines anterior-posterior polarity of the early mouse embryo. *Cell* **92**, 797-808.
Wilkinson, D. G. (1992). *In Situ Hybridization: A Practical Approach*, pp. 75-83. Oxford: IRL Press.
Wotton, D. and Massague, J. (2001). Smad transcriptional corepressors in TGF beta family signaling. *Curr. Top. Microbiol. Immunol.* **254**, 145-164.
Wotton, D., Lo, R. S., Lee, S. and Massague, J. (1999a). A Smad transcriptional corepressor. *Cell* **97**, 29-39.
Wotton, D., Lo, R. S., Swaby, L. A. and Massague, J. (1999b). Multiple modes of repression by the smad transcriptional corepressor TGIF. *J. Biol. Chem.* **274**, 37105-37110.